IARJSET ISSN (O) 2393-8021, ISSN (P) 2394-1588

International Advanced Research Journal in Science, Engineering and Technology

Impact Factor 7.105 ⁑ Vol. 9, Issue 3, March 2022

DOI: 10.17148/IARJSET.2022.9328

A Study of Effect of ECAP die angle on the strain homogeneity, microstructural evolution, crystallographic texture and mechanical properties of Pure Magnesium

Nagendra Singh[1*], Dr. Manoj Kumar Agrawal[2], Sanjeev Kumar Verma[3], Ashish Kumar Tiwari[4]

[1]Research Scholar Dept. of Mechanical Engineering. G.L.A .University, Mathura, INDIA

[2]Dept. of Mechanical Engineering. G.L.A .University, Mathura, INDIA

[3]Dept. of Mechanical Engineering. J.S .University, Shikohabad, INDIA

[4]Dept. Of Advanced Centre for Material Science. Indian Institute of Technology, Kanpur, INDIA

Abstract: Molecular dynamics was used to analyze the deformation behavior and polycrystal development of single-crystal aluminum during equal channel angular pressing (ECAP). At 320 K, an ECAP die with a curvature angle (Ψ) of 20^0 and a channel angle (φ) of 90^0 processed three samples with various beginning crystallographic orientations. The samples were orientated so that the extrusion direction was parallel to the [100], [110], and [111] directions (ED). Due to the strong compression force, shear strain was the major mechanism of deformation during ECAP, with normal strain present before entering the deformation zone. The sample oriented along the ED in the [100] direction had substantial grain fragmentation, the largest lattice rotation, but the lowest dislocation density and shear strain, whereas the sample orientated in the [111] direction had the opposite findings. The number of active slip systems, the quantity of shear strain, and grain rotation angle were all shown to be related, with the majority of lattice rotation occurring in the transverse direction. In addition, the deformation and grain fragmentation mechanisms that take place in the deformation zone were studied. Finally, the model may give findings that are similar to those found in the literature through experiments. For 4-passes of route Bc at 235^0C, pure Mg billets were treated utilizing two ECAP dies with internal channel angles of 90^0 and 120^0. The texture weakened in intensity after 1-Pass and 2-Passes, resembling the B fiber texture of optimum orientation {0001} <uvjw>. When the number of ECAP passes was increased to four, the result was a significant strong texture with more than 26 times the randomness of the intense {0001} poles.

Keywords: Pure Magnesium; Severe plastic deformation; Equal channel angular pressing Die angle; Microstructural evolution; Crystallographic texture.

1. INTRODUCTION

With the expansion of the aerospace and aeronautics industries, the demand for light and strong materials has increased [01], and researchers have begun exploring for novel alloys and ways to improve the physical and mechanical properties of materials and submicron grain refinement capabilities [02]. The SPD methods have been utilised to make ultrafine-grained (120-520 nm) and nanocrystalline (120 nm) materials, as well as to adapt materials for specific applications, in comparison to coarse-grained materials, nanocrystalline materials have increased strength, hardness, diffusivity, improved ductility/toughness, lower density, lower elastic modulus, higher electrical resistivity, increased specific heat, higher thermal expansion coefficient, lower thermal conductivity, and superior soft magnetic properties [03]. It has been a popular SPD method for bulk producing ultrafine-grained to nanocrystalline materials. In recent investigations, ECAP was found to improve galvanic corrosion resistance by more than 55% and stress corrosion cracking was found to be reduced after ECAP [04]. Other investigations have revealed yield strength and ultimate tensile strength improvements of more than 75% after multi-pass ECAP. MD is a strong technique that enables for detailed dynamic analysis of atomistic mechanisms and improved flexibility, both of which are challenging to do experimentally. MD simulations can also be utilised to investigate the deformation and process of ECAP at the atomic level. As a result, the use of MD is required to fully comprehend grain refining during ECAP. During deformation, dislocations occur and collect in metals. On the other hand, [05] found that raising the strain in ECAP of Al and Cu samples enhanced dislocation density up to a threshold of diminishing returns, after which additional strain increases resulted in dislocation density reduction. Furthermore, found

IARJSET ISSN (O) 2393-8021, ISSN (P) 2394-1588

International Advanced Research Journal in Science, Engineering and Technology

Impact Factor 7.105 ⋇ Vol. 9, Issue 3, March 2022

DOI: 10.17148/IARJSET.2022.9328

that active slip systems greatly controlled lattice rotation and dislocation structure in aluminium during deformation, and that the grain's crystal orientation was the key parameter governing the slip systems. Furthermore, numerous researchers observed that grain fragmentation occurred during plastic deformation, and that crystal orientation had a substantial influence. Therefore, The effect of crystal orientation on dislocations, deformation behaviour, and lattice rotation is critical to understand. The deformation behaviour and poly-crystallization during ECAP of single-crystal aluminium were explored using an MD simulation in this study [06].

Due to their strength-to-weight ratio, magnesium alloys (Mg alloys) are ultra-light alloys; for example, their density is two-thirds that of aluminium and one-quarter that of steel, In addition, Mg alloys have unique features such as high particular strength, specific making them appealing materials for a variety of applications in the aerospace and automotive industries. Furthermore, Mg alloys are regarded as a critical answer for reducing carbon dioxide emissions from vehicles, as they save roughly 15% in weight, which reduces fuel consumption by 10 to 15%. Nevertheless, The low formability of magnesium alloys is a key drawback that prevents them from being used in numerous industries, including aircraft and shipbuilding [07]. The lack of formability is due to the hexagonal close-packed (hcp) crystal structure of Mg, which limits the number of deformation modes possible. Forming Mg and related alloys using typical methods such as extrusion and rolling at room temperature fails. On the other hand, At higher temperatures, magnesium alloys can be deformed; however, dynamic recrystallization and recovery processes minimise the hardening effects of deformation. Several efforts over the last decade have resulted in the development of several types of magnesium alloys with a mix of ductility and strength, the formability of Mg alloys by applying plastic processing techniques to control texture is a desirable approach [08]. Sever plastic deformation (SPD) methods are promising approaches for processing Mg alloys at room temperatures. ECAP is one of the SPD techniques that is not only effective in producing nanostructure and UFG structure in alloys but also suitable to industry. Due to the association between the mechanical and microstructure properties of the deformed materials and the plastic deformation degree, various researchers have explored different characteristics of the ECAP process to investigate the impact of process parameters on material behaviour. As a result, in ECAP process design, understanding the phenomenon of strain development is critical. Eq. (1) shows the theoretical equivalent strain in relation to the die geometry [09]. The number of passes (N), the internal channel angle (φ), and the outside corner angle (Ψ) are the key elements impacting the strain on the ECAPed sample, as shown in Eq. (1). The ECAP die angles φ and Ψ are shown in Fig. 1.

$$\varepsilon_{eq} = \frac{N}{\sqrt{3}}\left[2\cot\left(\frac{\varphi+\Psi}{2}\right) + \Psi\mathrm{cosec}\left(\frac{\varphi+\Psi}{2}\right)\right] \qquad (1)$$

Over the last few years, For metal forming simulations, the finite element method (FEM) has proven to be the most reliable computer-aided analysis tool. Several studies involving ECAP processing parameters have been carried out using FEM, with the majority of their numerical analysis focusing on the influence of the φ value on deformation patterns and homogeneity. [10], investigated the effect of changing the φ value in the range from 0^0 to 90^0. Using finite element simulations with φ up to 90^0 for recreating the sharp angle, they discovered that the round angle caused inhomogeneous deformation. They discovered that as a result of the increased strain induced longitudinally on the sample's outer corner, a decrease in resulted in an increase in punch pressure. Furthermore, The strain is immediately affected by the ECAP pathways, resulting in massive changes in texturing, microstructures, and mechanical characteristics. The route BC displayed the most severely uniform distribution of strain after the third pass in the cross-sectional region, in contrast to route A, where the strain was concentrated at the top-left zone and route C around the corner.

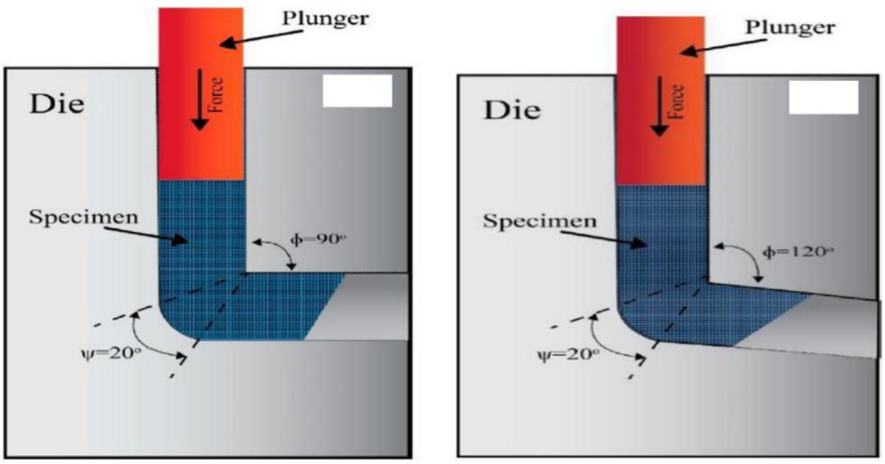

Fig. 1-Schematic of the ECAP dies with internal channel angle of (a) 90^0 and (b) 120^0 .

DOI: 10.17148/IARJSET.2022.9328

Because of textural development and ultra-grain refinement, it is well known that ECAP elongates and strengthens Mg alloys. Furthermore, Different ECAP processing routes with many passes were shown to have the greatest impact on grain refinement and to be the cause of frequent changes in direction and shear plane throughout the process [11]. In addition, Because of the non-basal slipping systems activation and the newly generated texture, the compressive mechanical characteristics of extruded pure Mg treated by ECAP at room temperature with $\varphi = 90^0$ and route B_C were shown to diminish after two passes. However, Due to grain refining, the mechanical characteristics improved after the fourth pass. Unfortunately, due to its weak deformation ability, research on pure Mg has been limited, with most studies focusing on Mg alloys with a tensile strength of φ of $\leq 90^0$. Consequently, The fundamental mechanism of recrystallization, hardening effects, and processes that limit grain size reduction were investigated using ECAP processing of pure Mg. In this study, FE simulation was used to investigate the influence of ECAP die angle and number of processing passes on the deformation behaviour and strain homogeneity of pure Mg. Furthermore, scanning electron microscopy (SEM) coupled with the EBSD technique was used to conduct a detailed examination of the impact of the ECAP procedure on crystallographic texture and microstructural evolution.The microstructural evolution and FE simulation were associated with the tensile characteristics and Vicker's microhardness values.

2. EXPERIMENTAL METHODS OR METHODOLOGY

2.1 Insert direction (ID), transverse direction (TD) and extrusion direction (ED):

To simulate a nano-ECAP environment, an MD simulation was undertaken using the LAMMPS. Three single-crystal aluminium samples with dimensions of 25 nm x 25 nm x 55 nm were employed, with various orientations along the extrusion direction (ED). The MD setup utilising a die with an of 20^0 and an of 90^0 is shown in Fig. 2, where AOB is the deformation zone, OC is the shear plane, and the shear direction is parallel to OC. To minimise the number of atoms in the system and thus save computational time, the die was established as a rigid body and made one atom thick. The [100] direction was parallel to the ED, and the [010] direction was parallel to the insert direction in the 100-sample (ID). Subsequently, The [110] direction was parallel to the ED and the $[1\bar{1}0]$ direction was parallel to the ID in the 110-sample, whereas the [111] direction was parallel to the ED and the $[1\bar{1}0]$ direction was parallel to the ID in the 111-sample. To allow the sample to expand during equilibration and relaxation while minimising friction during compression, the ECAP die was constructed with a slightly larger cross-sectional area of 21 nm x 21 nm. The samples were equilibrated at 320 K for 45 ps before ECAP. The simulation was run in a conventional (NVT) ensemble, with N equaling the total number of atoms in the system, V equaling volume, and T equaling temperature. Using the Nose-Hoover thermostat, the temperature was maintained at 320 K throughout the simulation. Compression was carried out at a rate of 2.5 A/ps with a timestep of 0.008 ps utilising an infinite mass piston.

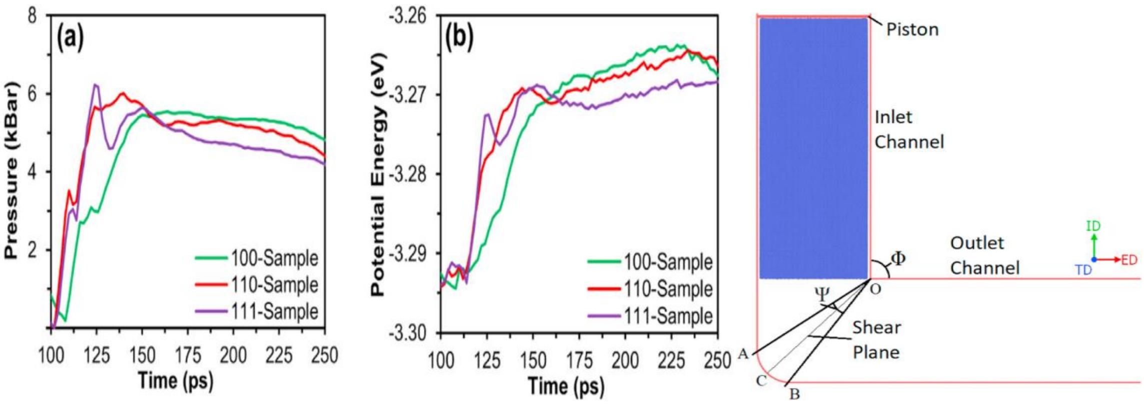

Fig. 2-The change of (a) pressure and (b) potential energy during ECAP for each sample and Insert direction (ID), transverse direction (TD) and extrusion direction (ED).

After 258 ps of ECAP, the samples were allowed to relax for 49 ps at 320 K. The embedded atom model (EAM) potential was used to calculate the interatomic potential. Elastic constants, phonon-dispersion curves, vacancy production, migration energy, stacking fault energy, and surface energy were all precisely recreated by the potential. As a result, this potential was appropriate for our research. The data were analysed using the Open Visualization Tool (OVITO) and polyhedral template matching (PTM) algorithms, and the following properties were investigated: the compression pressure throughout the extrusion process; the crystalline structure present after ECAP, such as grains, vacancies, and stacking faults; the magnitude of grain rotation when compared to the initial orientation; and the dislocation density and type.

IARJSET ISSN (O) 2393-8021, ISSN (P) 2394-1588

International Advanced Research Journal in Science, Engineering and Technology

Impact Factor 7.105 ⁘ Vol. 9, Issue 3, March 2022

DOI: 10.17148/IARJSET.2022.9328

2.2. Finite element analysis

The stress distribution and strain homogeneity along the sample's transverse and longitudinal sections (TS and LS) of pure Mg were investigated using FE analysis during ECAP processing. Simufactforming software version 13.3.1 by MSC software corporation was used to perform the FE under the same experimental conditions (processing at 235 C via route B_c). The ECAP process was simulated using the worm extrusion module. As illustrated in Fig. 3, the model included a die with two parts, a plunger, and ECAPed billets. Except for the Mg samples, which were visible during the simulation to improve and explain visualisation. Furthermore, the modelled plunger and 2-half die were discrete hard components composed of a fictitious nonformable substance. Based on the degree of distortion and the mesh sensitivity study, the mesh type was hexahedral mesh with a varied number of nodes from 9500 to 15,000 elements. Due to the deformation of the ECAPed billets, the experimental component employed the identical dimensions of the ECAP die and sample with particular caution. The positioning feature of the software was used to simulate the B_c route, with the last step of each pass being considered the first for the next pass. The components became overly skewed during ECAP simulation, necessitating a revision of the mesh structure. Based on a 1.2 mm element size and a 0.2 mm strain change, remeshing criteria were applied. The ECAPed material was modelled using both isotropic linear elastic and strain hardenable rigid-plastic modes. The tracked elements were found on the specimen's plane in the middle, on the edge where most strain occurred and in the centre, where ECAP has the least influence. The ram speed was set at 0.08 mm/s, which was the same as the experimental ram speed. At m = 0.08-0.2, the coefficient of friction performed well [12]. The die friction factor was set to 0.08 in the Coulomb friction model. The Mg strain hardening exponent and yield constant, which are both temperature and strain rate dependent, were calculated using a software-built tabular flow curve model.

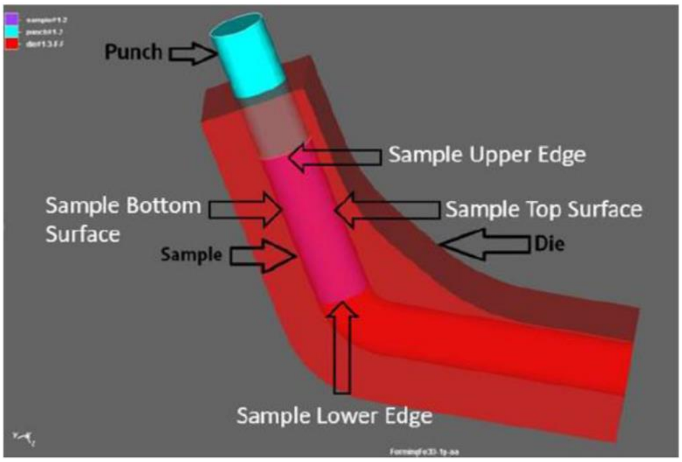

Fig. 3-The ECAP components used in FE simulation (El-Shenawy M, 2021).

2.3. Experimental procedure:

Commercial pure Mg (0.06 percent Al, 0.008 percent Ca, 0.005 percent Cr, 0.002 percent Cu, 0.015 Fe, 0.012 percent Mn, 0.005 percent Ni, and 0.06 percent Zn, with the rest being Mg) was used in this investigation, and it came in the form of 22 mm diameter rolled billets with 510 mm length. To make the ECAP samples, the pure Mg billets were sectioned into 62 mm lengths using a precision cutting machine. The samples were annealed at 255°C for 1 hour before ECAP processing, then cooled in the furnace. The pure Mg billets were processed through ECAP through 1, 2, and 4 passes of route B_c (1-P, $2B_c$, and $4B_c$), rotating the ECAPed billets by 90^0 degrees in the same direction after each processing pass. The ECAP process was carried out at a temperature of 255°C and a ram speed of 0.05 mm/s. Before each pass, a graphite-based lubricant was applied to reduce friction between the die's inner walls and the ECAPed samples. We utilised a split ECAP die with a 20^0 outer corner angle (Ψ). The two ECAP dies that were employed had internal channel angles (φ) of 90^0 and 120^0, respectively, as illustrated in Fig. 4. Based on Eq. 1, the equivalent strain of ECAP dies was 1.084 and 0.834 per pass, respectively (1). SEM was used to examine the microstructural evolution of commercial pure magnesium billets. In addition, before and after ECAP processing, EBSD was employed to investigate the structural evolution and crystallographic texture of Mg billets. The as-annealed sample (AA) and ECAP processed billets were used for microstructural characterization. The billets were cut along their longitudinal cross-section (LS) on a plane parallel to the pressing direction (flow plane) and perpendicular to the die entry channel, where the axes of the reference system coincide with the extrusion ECAP direction (ED). A conductive epoxy was used to mount the specimen cold. Grinding and polishing were done with rotating wheels at a rotational speed of 180 rpm. Between each grinding phase, the specimen was washed with water and ground with 610, 810, 1010, and 1210 silicon carbide papers. Polishing was done using diamond suspensions of 3.5 µm and 1.5 µm particle size with yellow DP-lubricant, and the last polishing step was done with a 0.08 µm particle size colloidal silica suspension until an optical microscope revealed a scratch-free

IARJSET ISSN (O) 2393-8021, ISSN (P) 2394-1588

International Advanced Research Journal in Science, Engineering and Technology

Impact Factor 7.105 ⪫ Vol. 9, Issue 3, March 2022

DOI: 10.17148/IARJSET.2022.9328

surface. As a lubricant, distilled water was employed. Between each polishing process, the specimen was ultrasonically cleaned in ethanol for 12 minutes and completely dried. Following polishing, the specimen was etched for a few seconds with a hydrochloricenitric acid solution (12 ml HCl + 8 ml HNO_{3-} + 100 ml ethanol) and immediately rinsed with ethanol. The specimen was ion milled for 35 minutes with a 2 keV ion beam energy, 0.425 s^{-1} specimen rotational speed, and an 85^0 specimen tilt angle (sample surface at 5^0 relative to the ion beam axis) using a flat ion milling machine to remove the etching stains or oxide layers from the surface. The EBSD measurements were carried out on the top surface of the ED plane with an SU-70 SEM at 18 kV, 1.8 nA typical current, and a 70^0 tilting angle. Using the HKL Channel5 Flamenco programme, crystallographic data was acquired with a 100-nm step size. Using the post-processing HKL Channel5 software, an inverse pole figure (IPF) map was created after the crystallographic data were gathered. Before and after ECAP processing, Vicker's microhardness tests (HV) were performed on the sample, commencing at the billets' peripheries and working inwards. The hardness test was performed for 18 seconds with a 0.8 kg applied weight. Furthermore, at room temperature, the tensile characteristics of ECAPed samples were tested using a 100 kN universal testing equipment with a strain rate of 10^{-3} s^{-1}. The specimens for the tensile tests were chosen from the middle of the ECAPed samples. Tensile samples were measured according to the E8M/ASTM standard. To guarantee the accuracy of the data, three tensile specimens per processing condition were evaluated.

3. RESULTS AND DISCUSSION

3.1. Compression pressure:

Figure 2a depicts the changes in pressure over time during ECAP. When the sample was compressed between 110 and 135 ps while in contact with the curvature of the die, the pressure grew dramatically to the point where extrusion began. During compression, both the 110-sample and the 111-sample showed comparable tendencies, with a rapid increase in pressure followed by a drop. The pressure reduction in the 111-sample was abrupt, but the pressure decline in the 110-sample was gradual. Aside from having the largest initial pressure peak, the 111-sample had the lowest pressure throughout ECAP, followed by the 110-sample. Throughout the ECAP procedure, the 100-sample had the slowest pressure growth but the highest compression pressure. Figure 2b depicts the average potential energy during ECAP, which displays a similar trend to the pressure change.

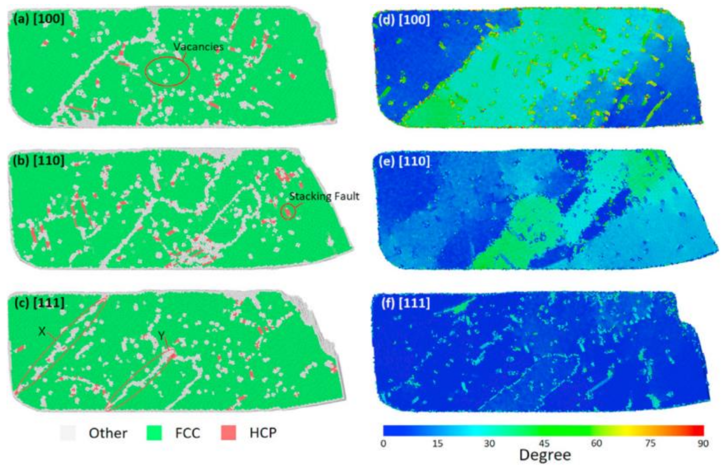

Fig. 4-The crystal structure present after ECAP showing stacking faults and vacancies: (a) 100-sample, (b) 110-sample (c) 111-sample; The degree of lattice rotation present after ECAP: (d) 100-sample, (e) 110-sample, (f) 111-sample.

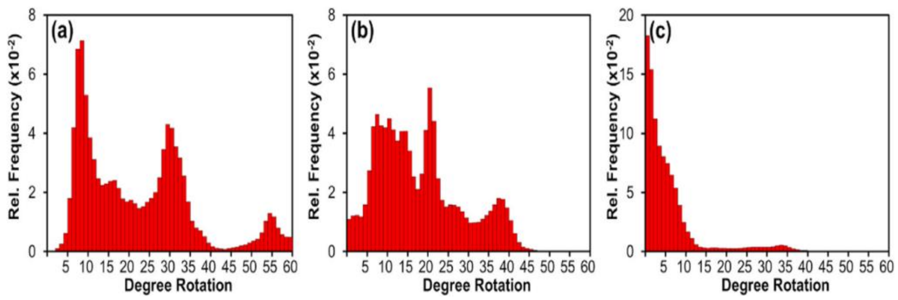

Fig. 5-Histogram of lattice rotation after one-pass ECAP:(a) 100-sample, (b) 110-sample, (c) 111-samples.

IARJSET ISSN (O) 2393-8021, ISSN (P) 2394-1588

International Advanced Research Journal in Science, Engineering and Technology

Impact Factor 7.105 ⁙ Vol. 9, Issue 3, March 2022

DOI: 10.17148/IARJSET.2022.9328

3.2. Crystal structure:

The crystal structure of the samples was largely a face centre cubic (FCC) structure, with some hexagonal close-packed (HCP) structure and "other configuration". An unknown coordination structure, such as an amorphous solid, grain boundary, or vacancies, was characterised as "other configuration." The HCP atoms correlate to stacking defects, which are created by the {111} plane slipping and twinning, whereas vacancies are created when a dislocation forces an atom to shift, leaving an empty place behind. The magnitude of lattice rotation computed by comparing the crystal orientation before and after ECAP. Because that region was not subjected to deformation, the lattice rotation was focused towards the centre of the sample, with essentially little lattice rotation at the bottom right and top left corners, which is a known behaviour during ECAP. The bottom right corner of the 110-sample exhibited modest lattice rotation, with the majority of the rotation occurring in the sample's centre. The 111-sample, on the other hand, showed very little lattice rotation, albeit the shape of a few grains could be observed. With a misorientation angle of 3^0 and 8^0, respectively, the X and Y limits indicated is played modest misorientation across the boundaries. The X and Y grain boundaries were designated as low-angle grain barriers since the misorientations were less than 15^0. A histogram of the lattice rotation angle for all samples is shown in Fig. 5. The highest degree of rotation was found in the 100-sample, with more than 15% of atoms undergoing a high-angle rotation of 55^0 or more. Furthermore, the 110-sample, like the 100-sample, exhibited a high degree of grain rotation, with the exception of a maximum rotation of 45^0, with the majority of the samples rotating between 10^0 and 25^0. The 111-sample, on the other hand, showed the least degree of rotation, with almost 95% of the sample undergoing a rotation of 10^0 or less. Experiments with a single-crystal Al sample treated with a die of the same geometry yielded similar results.

3.3. Dislocation analysis:

Figure 5 depicts a snapshot of the dislocations present in a small cross-section of the 111-sample after ECAP, highlighting the many types of dislocations that can be seen following a single-pass ECAP. Shockley dislocations were found to be the most common type of dislocation surrounded by HCP atoms, while Stair-Rod and Hirth dislocations were found to be less common. Shockley dislocations were found in large concentration on the Y line, while Perfect and Shockley dislocations were found on the X line. Furthermore, Stair-Rod dislocations were predominantly visible on the white patches in Fig. 6, which matched to the existence of vacancies or a multi dislocation node. The 100-sample and the 110-sample both have similar dislocation characteristics. Around grain borders, the sample showed a significant concentration of Shockley and Perfect dislocations, as well as the production of HCP structures caused by the dissociation of Perfect dislocation into paired Shockley dislocation at grain boundaries. Figure 6 depicts the evolution of dislocation density for all samples during the ECAP process, including overall dislocation density as well as Shockley and Perfect dislocation densities, with Shockley dislocations accounting for the majority of the dislocations. In comparison to the other samples, the 100-sample had a moderate increase of dislocations and the lowest dislocation density at the peak. The dislocation density in the 110-sample increased rapidly at the start of the ECAP process, then plateaued with a tiny surge at the end. The 111-sample, on the other hand, exhibited the highest dislocation density, with the sample rising rapidly at first and continuing to climb throughout the ECAP procedure.

3.4. Strain analysis:

Figure 7 displays a snapshot of the 110-sample taken at 165 ps during ECAP. The shear strain angles recorded for the 100-sample, 110-sample, and 111-sample were 26.9^0, 25.4^0, and 22.1^0, respectively, resulting in shear strains of 2.16, 2.30, and 2.69, according to Eq (2).

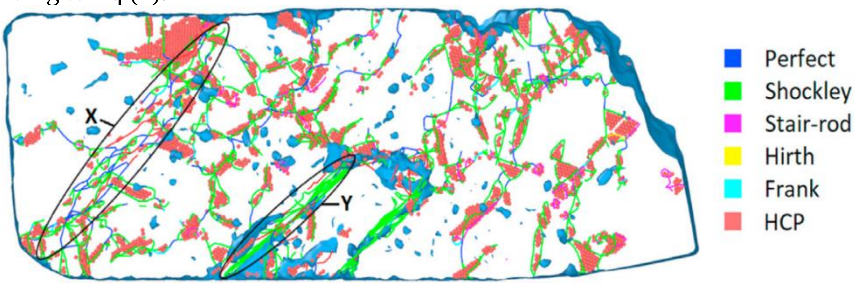

Fig. 6-50 A slice shows the different dislocations present after a one-pass ECAP for the 111-sample.

When the crystal split into two parts in the deformation zone, the grain boundary was established. The grain boundary was generated at an angle of $\Phi/2$, or 45^0 with the ED crossing the boundary with an amisorientation angle of 5^0. The largest shear strain was recorded near the grain boundary, which was surrounded by shear bands, Because of the high shear stress in the deformation zone, shear bands formed parallel to the FCC slip direction, i.e., the <110> direction. Shear bands were localised around the grain boundary. The dislocations and HCP structure formed, and the HCP structure matched to the slippage or twinning of the {111} plane, resulting in stacking faults. The defect mesh (blue mesh) also

DOI: 10.17148/IARJSET.2022.9328

indicated the surface of the grains in the sample, as well as dislocation cores and other defects like grain boundaries. The development of two new grains could be regarded as the existence of the faulty mesh at the place of grain splitting, at the site of grain splitting, as shown by the creation of red bands roughly Φ/2, or 45^0, with the ED.

3.5. Strain Analysis:

ECAP was previously thought to be a simple shear deformation mechanism that occurs in the deformation zone (Segal VM, 1999, Iwahashi Y, 1996 and Pardis N, 2017). Eq. (2) may be used to compute the theoretical shear strain (Iwahashi Y, 1996) obtained following a one-pass ECAP:

$$\gamma = 2\cot\left(\frac{\Phi+\Psi}{2}\right) + \Psi\csc\left(\frac{\Phi+\Psi}{2}\right) \qquad (2)$$

where Φ is the die angle, and Ψ is the angle of curvature. The theoretical shear strain and q were estimated to be 1.88 and 28.78, respectively, for die with Φ of 90^0 and Ψ of 20^0. Equation (3) can be used to compute the actual shear strain encountered following one-pass ECAP:

$$\gamma = \tan(90^0 - \theta) \qquad (3)$$

where θis the angle between the sheared element and ED. Fig. The deformation of a 30 Å x 30 Å piece in the 100-sample and 111-sample is shown in Fig. 8. The element was chosen in the middle of the sample and followed through ECAP. Before approaching the deformation zone at 195 ps, the components were squeezed and partially sheared (Fig. 9). The element was constantly sheared once it entered the deformation zone until it exited the deformation zone. Similarly, the 110-samples yielded similar results. The ID of the 100-sample and 111-sample samples were compressed by 5 Å and 6 Å correspondingly, corresponding to a normal strain of 0.20 and 0.35, respectively. The samples were compressed due to enormous compression forces during extrusion, whereas the element's slight shear before entering the deformation zone could be attributed to the element's interaction with the continuous movement of atoms below, which applied a shear force in the ED, similar to a viscous fluid flowing through a pipe. Furthermore, because the grains glided on one another once they split, shear before the deformation zone was reduced.

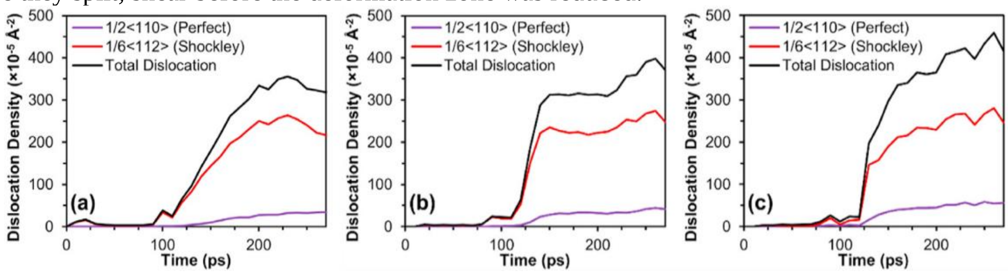

Fig. 7-Plots of dislocation density during ECAP showing Perfect, Shockley and total dislocation: (a) 100-sample, (b) 110-sample (c) 111-sample.

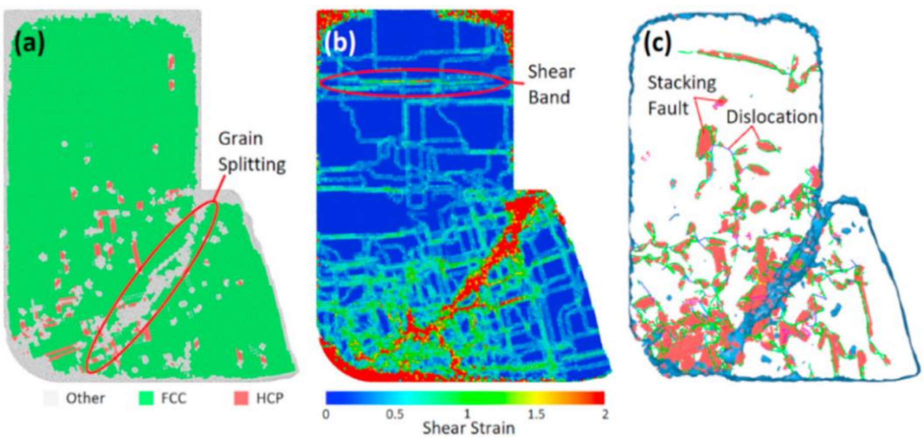

Fig. 8-ECAP of 110-sample at 160 ps showing grain splitting and formation of grain boundary; (a) The crystal structure; (b) The shear strain; (c) The dislocations and stacking faults.

3.6. Shear factor:

At the beginning of ECAP, all samples were compressed, as shown in Fig. 9. As a result, the increase in pressure from the simulation start to 128 ps is most likely attributable to compression (Fig. 2a). When compressive/tensile tests are performed on metals, Schmid's law states that the critical resolved shear stress is determined by multiplying the cosine of the angle with the vector normal to glide plane and the cosine of the angle with the glide direction. The deformation of a 30 Å x 30 Å element throughout ECAP showing compression and shear; (a) 100-sample, (b) 112-sample.

IARJSET ISSN (O) 2393-8021, ISSN (P) 2394-1588

International Advanced Research Journal in Science, Engineering and Technology

Impact Factor 7.105 ⁘ Vol. 9, Issue 3, March 2022

DOI: 10.17148/IARJSET.2022.9328

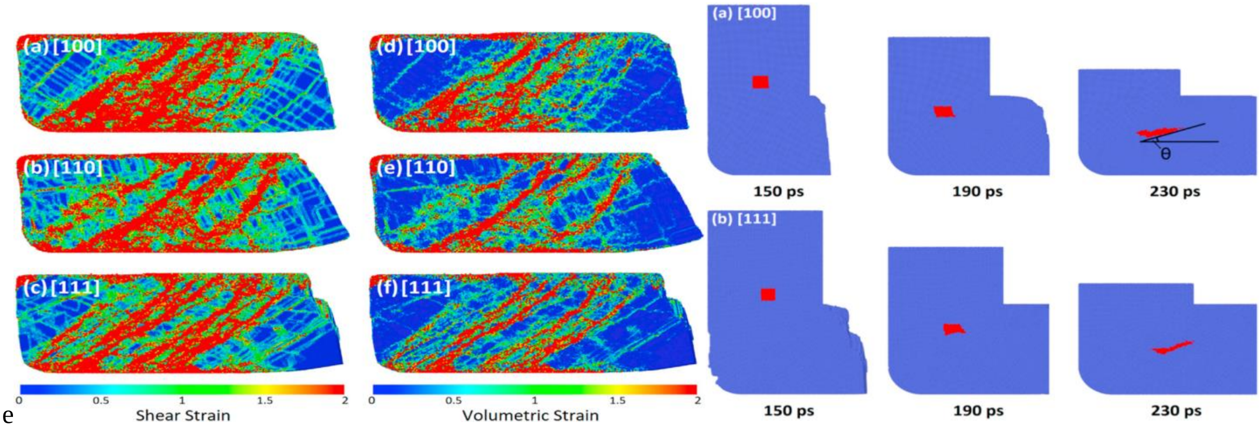

e

Fig. 9-The shear strain present after ECAP: (a) 100-sample, (b) 110-sample (c) 111 sample; The volumetric strain present after ECAP: (d) 100-sample, (e) 110-sample, (f) 111-sample.

3.7. Mechanical properties:

The homogeneity of hardness distribution over the perimeter and central areas of the ECAPed billets was assessed using Vicker's microhardness test. Figure 10 shows the hardness variations of Mg billets processed through ECAP dies with internal channel angles of $\varphi = 90^0$ and 120^0 as a function of the number of passes along route B_c.

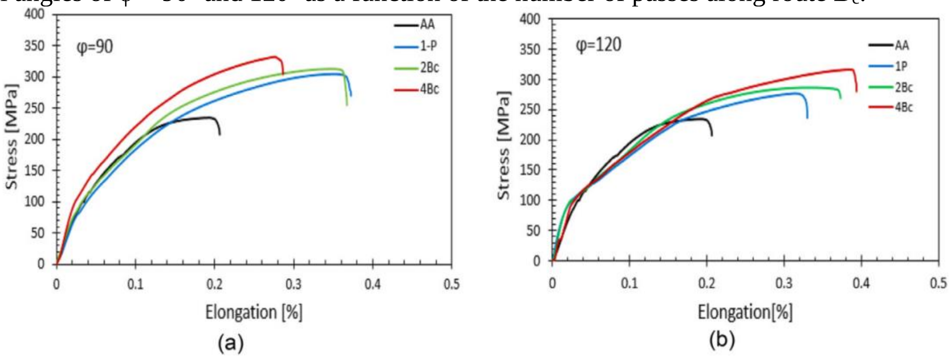

Fig. 10-Tensile stressestrain curves of Mg billets processed through ECAP using the 90^0-die and 120^0-die via 1-P, $2B_c$, and $4B_c$.

The as-annealed Mg had an average hardness of 28 HV. The hardness of AA-Mg increased dramatically as the number of ECAP passes increased in both the central and peripheral areas, as shown in Fig. 10. Furthermore, in both the central and peripheral regions, the 90^0-die had greater HV values than the 120^0-die. In comparison to the AA equivalent, processing through 1-P employing the 90^0-die resulted in a considerable increase in HV of 58% and 88 percent at the central and peripheral areas, respectively. This might be due to direct contact between the sample and the die walls, which resulted in more grain refining and more strain hardening, raising the hardness relative to the central regions, which is consistent with the FE results in Fig. 8. In comparison to the same condition of the 120^0-die, the 1-P condition of the 900-die exhibited an increase in HV of 15% and 21% at the central and peripheral regions, respectively, as shown in Fig. 19. The increase in HV values as the internal die angle is reduced can be attributed to an increase in plastic strain during ECAP processing, which is consistent with the FE findings. Furthermore, compared to the 1-P equivalent, processing through $2B_c$ employing the 90^0-die resulted in a 13.8 percent and 6.35 percent increase in HV at the central and periphery areas, respectively. The $2B_c$ condition of the 120^0-die showed a similar pattern. When the plastic strain was increased to 4Bc utilising the 90^0-die, the HV at the central and peripheral portions increased by 79 percent and 118 percent, respectively, when compared to the AA equivalent. In comparison to the 120^0-die counterparts, the $4B_c$ condition of the 90^0-die showed an increase of 9.7% and 8.8% in HV-values at the central and peripheral areas, respectively. This can be attributable to the grain refining that happened, as seen in Table 1, where the averaged grain size at the $4B_c$ for the 90^0-die and 120^0-die, respectively, was 0.98 and 1.98. Furthermore, strain hardening during ECAP processing aided in the growth of HV-values when the number of passes was increased. Tensile tests were performed on Mg billets before and after ECAP processing at 225°C using 1-P, $2B_c$, and $4B_c$. Figure 9 shows the stressestrain curves of the ECAPed samples. Fig. The processing of Mg billets using both 90^0-die and 120^0-die had no significant influence on yield strength, which contradicts the standard Hall-Petch relationship, which indicates that lowering grain size increases yield strength. As can be observed in Figs. Increasing the number of ECAP passes to 9, 10, and 13 resulted in a considerable reduction in grain

IARJSET ISSN (O) 2393-8021, ISSN (P) 2394-1588

International Advanced Research Journal in Science, Engineering and Technology

Impact Factor 7.105 ⪤ Vol. 9, Issue 3, March 2022

DOI: 10.17148/IARJSET.2022.9328

size. Earlier this year, similar findings were published in [13]. The 1-P showed a significant improvement in both ultimate tensile strength (UTS) and elongation (EL) by 35 percent and 95 percent, respectively, as shown in Fig. 10 ($\varphi = 90^0$). The UTS increased by 7% when the strain was increased to $2B_c$, however the EL reduced by 8% when compared to the 1-P. In comparison to the $2B_c$ counterpart, increasing ECAP passes to 4Bc resulted in a 15% gain in UTS and a 25% drop in EL. 1-P at $\varphi = 120^0$, on the other hand, exhibited a significant rise in UTS and EL of 14.8 percent and 68 percent, respectively. As ECAP passes were increased to $2B_c$, the UTS increased by 8%, with an insignificant increase of 15% for EL, when compared to the 1-P counterpart. In the 4Bc condition, both UTS and EL improved by 12% and 7%, respectively.

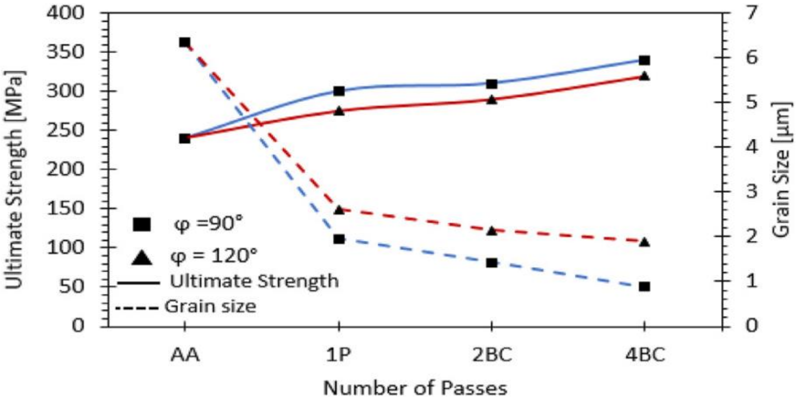

Fig. 11-Variation of UTS and grain size of Mg billets processed through ECAP dies with channel angles of 90^0 and 120^0 with respect to the number of passes.

With increasing the ECAP deformation passes, the tensile results were consistent with the relative increase in HABs and grain refinement (Figs. 10 and 11). The increase in UTS can be attributed to the texture intensity increasing in tandem with the amount of ECAP passes. As a result, the strain accumulated. Furthermore, increasing the HABs in the ECAP process resulted in the production of ultra-fine grained materials. In comparison to 120^0 counterparts, utilizing $\Psi = 90^0$ resulted in finer grain size of ECAPed Mg billets, resulting in higher UTS. The decrease in ductility observed in $\Psi = 90^0$ as the number of passes increased might be attributed to the lower grain size, as a smaller grain size increases the grain boundary area per unit volume, causing material strengthening to increase and ductility to decrease. In a prior study, similar conclusions were reported. The 120^0-die, on the other hand, showed higher ductility than the 90^0-die, which could be attributed to the lower strain experienced when using the 120^0 angle die compared to the 90^0, which is consistent with the FE findings in Fig. 8. As a result, the bulk materials in 120^0-die indicated the existence of bimodal and dynamic recrystallization grains (DRX), which helped to improve ductility [14]. Furthermore, the grain size at the $4B_c$ was varied between 0.21 m and 7.14 m using the 90^0-die and 0.81 m and 25.15 m using the 120^0-die, as shown in Table 1. The fine grains, which are less than 8 m in length, were reported to have great strength; however, the lager grains, which are around 28 m in length, offered strain hardening to sustain the deformation of huge stresses. As a result of the unique textures, which favor grain sizes in the 18-25 m range and basal slip, the ductility of ECAPed Mg billets improved, which is consistent with the findings found. Furthermore, the ECAPed billets' improved ductility compared to the AA condition could be related to the bimodal grain structure's ease of dislocation moments [15].

The lower the critical shear stress, the larger the Schmid's factor. The Schmid factor of the 111-sample is predicted to be slightly lower than that of the other samples, with values of 0.40 and 0.41 for the 111-sample and 100-sample, respectively. As a result of the reduced Schmid's factor, the highest pressure peak occurs early in the process. Shear, on the other hand, distorted the sample after extrusion began. Because the starting crystal orientation influences the quantity of grain rotation and shear strain experienced by the samples, calculating the resolved shear stresses associated with the chosen orientation is vital. determined the angle between the sample's slip system, the theoretical shear plane, and the angle between them using Eq. (4):

$$\tau_{rss} = (F/A)\cos\alpha\,\cos\beta \qquad (4)$$

Where τ_{rss} is the shear stress acting on the slip plane, F is the force in the shear direction, A is the area of the shear plane, and $\cos\alpha\,\cos\beta$ is the shear factor ranging from 0 to 1, where α is the angle between the die's shear plane normal and the {111} slip plane normal while b is the angle between the shear direction and <110> slip direction.

The shear factor for each slip system is shown in Table 1. Six active slip systems are included in the 100-sample, two of which have a shear factor of 0.84: (111)[110] and (111)[110]. Eight slip systems with the identical shear factor of 0.42 are activated by the 110-sample. During ECAP, the 111-sample, on the other hand, triggered all of the slip systems. With a shear factor of 0.76, the 111-sample can readily activate the (111)[101] slip mechanism, considerably increasing the

IARJSET ISSN (O) 2393-8021, ISSN (P) 2394-1588

International Advanced Research Journal in Science, Engineering and Technology

Impact Factor 7.105 ⁜ Vol. 9, Issue 3, March 2022

DOI: 10.17148/IARJSET.2022.9328

shear strain. With more active slip mechanisms, the sample will quickly deform, resulting in increased strain. For the 111-sample.

Table 1 - The calculated shear factor with respect to the sample.

Slip Plane	Slip Direction	Shear Factor		
		100-sample	110-sample	111-sample
111	$\bar{1}01$	0.01	0.01	0.28
	$1\bar{1}0$	0.01	0.42	0.53
	$01\bar{1}$	0.01	0.42	0.28
$1\overline{11}$	101	0.41	0.00	0.75
	$\overline{11}0$	0.84	0.42	0.49
	$01\bar{1}$	0.42	0.42	0.31
$\overline{11}1$	101	0.01	0.01	0.24
	011	0.01	0.42	0.02
	$1\bar{1}0$	0.01	0.42	0.18
$\bar{1}1\bar{1}$	$\bar{1}01$	0.42	0.01	0.14
	$\overline{11}0$	0.84	0.42	0.22
	011	0.42	0.42	0.10

The shear factor differential, in combination with the number of active slip systems, explains why different beginning orientations result in varying shear strain magnitudes. revealed that a single-crystal Al sample with the same orientation as the 111-sample, processed in a die with the same geometry, was deformed without rotating during uniaxial compression, preserving the sample's crystal orientation. In addition, after uniaxial compression, the sample can slip in four different directions using two slip planes. This symmetrical slip is thought to be the reason for the crystal's homogenous deformation and lack of grain rotation.

CONCLUSION

After a one-pass ECAP, the deformation behavior and polycrystal formation of three aluminum single-crystals with varied beginning orientations were explored using an MD model to explain the deformation behavior and polycrystal formation, and the following conclusions were found.

1. Before entering the deformation zone, the samples were subjected to shear strain and normal strain due to compression. As a result, the shear strain exceeded the theoretical shear strain. The shear strain, on the other hand, was influenced by the original crystal orientation.
2. At the atomic level, the strain distribution and kinds present during ECAP were observed. Within the samples, the strain was distributed in an inhomogeneous (non-uniform) manner, with the shear strain dominating and the volumetric strain following the same pattern. Furthermore, the most strain was centered in the area where grain splitting took place.
3. The grain rotation angle, the magnitude of the shear strain imposed on the sample, and the dislocation density were all affected by the initial orientation, with the 111-sample having the highest shear strain and lowest lattice rotation and the 100-sample having the least shear strain and highest lattice rotation.
4. The 111-sample had the maximum strain and dislocation density with very little grain rotation and fragmentation, which was attributed to the sample's unique orientation, where the sample deformed through slip rather than grain rotation and fragmentation.
5. When compared to the other samples, the 100-sample had the most grain splitting and the most misorientation. As a result, the number of active slip systems, the misorientation angle, dislocation density, and grain fragmentation all have a strong link.
6. We're currently researching on the ECAP of body center cubic (BCC) and hexagonal close-packed (HCP) metals such a-iron and magnesium for future research. We also plan to research the ECAP technique for polycrystalline aluminum and compare it to the current findings.
7. In comparison to the 120^0-die, FE revealed that the 90^0-die had a more homogeneous distribution of the plastic strain.
8. The accumulation of plastic strain up to 4Bc in the 90^0-die and 120^0-die resulted in considerable refinement of 96 percent and 80%, respectively, compared to the as-annealed counterpart, according to EBSD analysis.

DOI: 10.17148/IARJSET.2022.9328

9. 4Bc of the 90^0-die produced a considerable strong texture with more than 26 times random, with the intense {0001} poles aligned in the middle of the TD and ED, whereas 4Bc of the 120^0-die produced a weaker texture with 13 times random.
10. The texture components were severely rotated due to the rotation of SPN and SD relative to the die angle during 1-P processing utilizing the 120^0-die, resulting in an extremely strong texture with around 23 times random.
11. As the plastic strain was increased to $4B_c$ utilizing the 90^0-die, the HV at the central and peripheral portions increased by 87 percent and 118 percent, respectively, when compared to the AA equivalent.
12. In comparison to the 120^0-die equivalent, the $4B_c$ condition of the 90^0-die showed an increase of 9.5% and 8.8% in HV-values at the central and peripheral regions, respectively.
13. ECAP processing through $4B_c$ resulted in a 48 percent and 44 percent increase in UTS of Mg billets treated in the 90^0-die and 120^0-die, respectively, as well as a considerable improvement in ductility when compared to the AA equivalent.
14. The yield strength of the Mg billets did not vary significantly after ECAP processing.

REFERENCES

[01] Junaidi Syarif, Amro Altoyuri, Intan Fadhlina Mohamed, Equal channel angular pressing of single crystal aluminum: a molecular dynamics simulation journal of materials research and technology 2022;17:888-897. https://doi.org/10.1016/j.jmrt.2022.01.061.
[02] Williams JC, Starke EA. Progress in structural materials for aerospace systems. Acta Mater 2003;51:5775-99. https://doi.org/10.1016/j.actamat.2003.08.023.
[03] Suryanarayana C. Structure and properties of nanocrystalline materials. Bull Mater Sci 1994;17:307-46. https://doi.org/10.1007/BF02745220.
[04] Sekar P, Sanna N, Desai V. Enhancement of resistance to galvanic corrosion of ZE41 Mg alloy by equal channel angular pressing. Mater Corros 2020;71:571-84. https://doi.org/10.1002/maco.201911337.
[05] Murata Y, Nakaya I, Morinaga M. Assessment of strain energy by measuring dislocation density in copper and aluminium prepared by ECAP and ARB. Mater Trans 2008;49:20-3. https://doi.org/10.2320/matertrans.ME200707.
[06] Larsen PM, Schmidt Sø, SchiØtz J. Robust structural identification via polyhedral template matching. Model Simulat Mater Sci Eng 2016;24. https://doi.org/10.1088/0965-0393/24/5/055007.
[07] Vijay Reddy K, Pal S. Structural evolution and dislocation behaviour during nano rolling process of FCC metals: a molecular dynamics simulation based investigation. J Appl Phys 2019;125:095101. https://doi.org/10.1063/1.5085750.
[08] A.I. Alateyah, Mohamed M. Z. Ahmed, Majed O. Alawad d, Sally Elkatatny, Yasser Zedan, Ahmed Nassef, W.H. El-Garaihy, Effect of ECAP die angle on the strain homogeneity, microstructural evolution, crystallographic texture and mechanical properties of pure magnesium: numerical simulation and experimental approach journal of materials research and technology 2022;17:1491-1511 https://doi.org/10.1016/j.jmrt.2022.01.088.
[09] Segal VM. Materials processing by simple shear. Mater Sci Eng, A Jul. 1995;197(2):157-64. https://doi.org/10.1016/0921-5093(95)09705-8.
[10] Nagasekhar AV, Tick-Hon Y, Li S, Seow HP. Effect of acute tool-angles on equal channel angular extrusion/pressing. Mater Sci Eng, A Nov. 2005;410(411):269-72. https://doi.org/10.1016/j.msea.2005.08.043.
[11] Shaeri MH, Salehi MT, Seyyedein SH, Abutalebi MR, Park JK. Characterization of microstructure and deformation texture during equal channel Angular pressing of AleZneMgeCu alloy. J Alloys Compd Nov. 2013;576:350-7. https://doi.org/ 10.1016/j.jallcom.2013.05.182.
[12] Alkorta J, Gil Sevillano J. A comparison of FEM and upperbound type analysis of equal-channel angular pressing (ECAP). J Mater Process Technol Nov. 2003;141(3):313-8. https://doi.org/10.1016/S0924-0136(03)00282-6.
[13] Fan GD, Zheng MY, Hu XS, Xu C, Wu K, Golovin IS. Improved mechanical property and internal friction of pure Mg processed by ECAP. Mater Sci Eng, A Oct. 2012;556:588-94.
[14] Naik GM, Narendranath S, Kumar SSS. Effect of ECAP die angles on microstructure mechanical properties and corrosion behavior of AZ80 Mg alloy. J Mater Eng Perform 2019;28:2610-9.
[15] del Valle JA, Carre~no F, Ruano OA. Influence of texture and grain size on work hardening and ductility in magnesiumbased alloys processed by ECAP and rolling. Acta Mater Sep. 2006;54(16):4247-59. https://doi.org/10.1016/j.actamat.2006.05.018.